Dominance formulation in multi-component binary phase equilibria

Daoyuan Qian,[1] Hannes Ausserwoger,[1] Tomas Sneideris,[1] Rohit Pappu,[2] and Tuomas P. J. Knowles[1,3,†]

[1] *Centre for Misfolding Diseases, Yusuf Hamied Department of Chemistry, University of Cambridge, Lensfield Road, Cambridge, CB2 1EW, UK*

[2] *Department of Biomedical Engineering and Center for Biomolecular Condensates, Washington University in St. Louis, St. Louis, MO 63130, USA*

[3] *Cavendish Laboratory, Department of Physics, University of Cambridge, J J Thomson Ave, Cambridge, CB3 0HE, UK*

Binary phase separation with conserved order parameters is a generic thermodynamic process that arises in different contexts. One system of great fundamental and practical interest is the condensation of bio-molecules, where the order parameters are concentrations of solutes, and the condensed phase typically contains many different components of diverse properties. In such systems, each solute species corresponds to one dimension in the full phase space and a major challenge in the field is to rigorously interpret and quantify the multi-component character of any given phase separation system. Here, we formulate a dominance parameter D^α for each solute α in a multi-component system, and show that it is easily accessible in experiments and relates to the underlying thermodynamics and the phase space. We complement the theoretical work with experimental data, and demonstrate that D^α reflects the interactions driving phase separation. A simple computational model further illuminates the variation of D^α across the whole phase space. This work paves the way for future quantitative investigations into multi-component systems.

The general principle of liquid-liquid binary phase separation is simple: starting from a single mixed solution state, the solutes de-mix to form two compartments with distinct compositions to lower the system's total free energy, and this free energy change is denoted by Δf. The two compartments formed have equal chemical potentials and osmotic pressure, as required by phase equilibria [1]. This process is the theoretical underpinning of bio-molecular condensate formation [2–4], which has been shown to play important roles in cellular physiology [5–9] and also diseases [10, 11]. Experimentally, the phase-separating macromolecule - typically a protein - is tagged by a florescent dye, and the protein concentration can be measured through fluorescence microscopy. As a result, it normally appears that the system forms a protein-rich dense phase and a protein-poor dilute phase, and the 1-D picture is often assumed [12–15]. This, however, is an over-simplification as many more solute dimensions are ignored, and the dilute and dense phases can differ not only in macromolecule concentration but also in pH [16] and salt concentrations [17], so important mechanistic information can be lost due to this oversight. Notably, the macromolecule polyethylene glycol (PEG) has traditionally been used by the bio-molecular condensate field as an inert crowder [11, 18] but it is increasingly clear that PEG is acting as an associative linker that partitions inside condensates [19–21], instead of staying in the dilute phase to exert an osmotic pressure.

A major challenge thus arises: how can one define, quantify, and measure, the multi-component character of such systems? Furthermore, solute species present in experiments have very different properties, for instance the molecular weight of a typical protein is of the order 100 kilodalton, while that of salt is of the order 100 dalton - how can these species be compared on an equal footing? This challenge calls for a dimensionless parameter defined for every solute in the same way, irrespective of their molecular details, that allows such comparisons to be made. Surprisingly, construction of such a parameter is easy from simple experimental data. Denoting the total concentrations of solutes to be ϕ^α where $\alpha = 1, 2, \ldots, N$, and suppose that the dilute phase concentration of solute 1, denoted as ψ^1_-, can be measured. A series of experimental samples can be prepared with varying ϕ^1 while keeping all other ϕ's constant and measuring ψ^1_-. This corresponds to traversing the phase space in a line parallel to the ϕ^1 axis and we term this 'homotypic line-scan' (Figure 1a). We take experimental data on phase separation of the optoG3BP1 protein in cells [22] where such a response curve is measured, treating the protein as solute 1 (Figure 1b). Denoting the gradient of the response $\frac{\partial \psi^1_-}{\partial \phi^1}$ as R^1_1, we trivially have $R^1_1 = 1$ outside the phase-separated region, and the response becomes modulated beyond some critical value ϕ^1_c. In an ideal 1-D system, for $\phi^1 > \phi^1_c$ we expect $R^1_1 = 0$, while because of the multi-component nature of the system [22] we have $R^1_1 > 0$ for optoG3BP1. We denote this deviation of R^1_1 at $\phi^1 > \phi^1_c$ from 1 as D^1, the dominance, with the index 1 implying a similar metric can in principle be measured for any other solutes. D^1 is defined as $D^1 \equiv 1 - R^1_1$, or more generally for a solute with index α,

$$D^\alpha \equiv 1 - R^\alpha_\alpha \tag{1}$$

where repeated greek indices are not summed in this manuscript. Using a 2-segment linear fit for optoG3BP1 data we obtain $D^1 = 0.55 \pm 0.14$. In contrast, in another system involving the protein optoFUS [23], the protein exhibits much more prominent single-component character (Figure 1c) and the dominance of optoFUS is

† tpjk2@cam.ac.uk

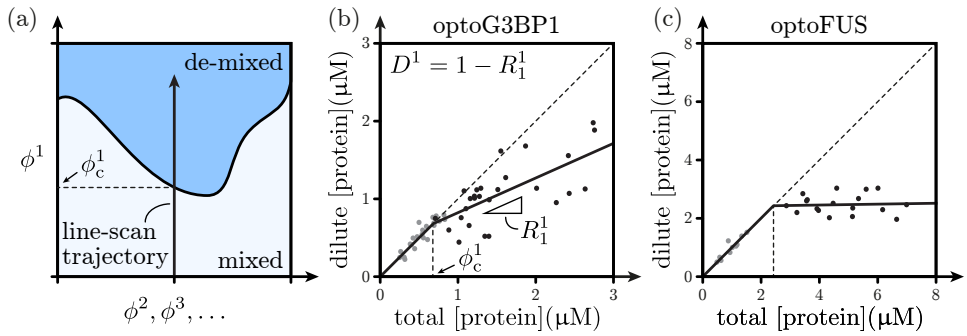

FIG. 1. **Dilute phase homotypic responses naturally define the dominance parameter.** (a) Illustration of the line-scan sampling method in a generic phase space. The dilute phase solute 1 concentration increases until the sampling enters the phase-separated region at $\phi^1 = \phi^1_c$, after which the increase becomes modulated by phase separation. (b) The dilute phase response of optoG3BP1 [22] exhibits multi-component character, with $D^1 = 1 - R^1_1 = 0.55 \pm 0.14$. (c) In the optoFUS system [23] the protein has much stronger single-component character. Scatter plot is data with black dots being phase separated and grey dots homogeneous. Diagonal dashed line is expected response without phase separation, and solid line is a 2-segment linear fit.

$D^1 = 0.98 \pm 0.07$. This is consistent with the observation that FUS phase separates easily on its own [13, 24] and can be less reliant on other components compared to G3BP1, where other macromolecules such as RNA are typically added to G3BP1 solution to trigger phase separation [8, 25]. D^α is thus an experimentally accessible quantity, and next we show that instead of an arbitrary construct, it reflects the structure of the phase space as well as the thermodynamic driving forces of phase separation.

In a generic N-D system, each point on the dilute phase boundary ψ^α_- is connected to another point on the dense phase boundary ψ^α_+, via a tie line vector $k^\alpha \equiv \psi^\alpha_+ - \psi^\alpha_-$. For a sample point ϕ^α within the phase separated region, the dilute and dense phase compositions that arise at equilibrium satisfy the condition that ϕ^α, ψ^α_-, and ψ^α_+ all lie on the same tie line, as required by mass conservation. The volume of the dense phase relative to the whole system is denoted as v, so $0 \leq v \leq 1$ and v represents the position of ϕ^α on the tie line k^α. The mass conservation condition is expressed as $\phi^\alpha = (1-v)\psi^\alpha_- + v\psi^\alpha_+$. Furthermore, the dilute phase boundary is an $(N-1)$-D surface and we use n_α to denote the vector normal to this surface. This construction of the phase space is entirely geometrical and the only assumption is that two phases co-exist at equilibrium (Figure 2a). It is easily shown via mass conservation that changes in ψ^α_- in response to changes in ϕ^α (Figure 2b), $\frac{\partial \psi^\alpha_-}{\partial \phi^\beta} \equiv R^\alpha_\beta$, can be expressed as (SI section I)

$$R^\alpha_\beta = \delta^\alpha_\beta - \frac{n_\beta}{n_\alpha}\left(\frac{n_\alpha k^\alpha}{\sum_{\gamma=1}^N n_\gamma k^\gamma}\right) = \delta^\alpha_\beta - \frac{n_\beta}{n_\alpha} D^\alpha \tag{2}$$

when evaluated on the phase boundary or if the tie lines are locally parallel. δ^α_β is the Kronecker delta and in the second equality we observe that by setting $\beta = \alpha$ and noting Eq. (1), the proposed dominance metric can be expressed as the geometrical quantity

$$D^\alpha \equiv \frac{n_\alpha k^\alpha}{\sum_{\gamma=1}^N n_\gamma k^\gamma} \tag{3}$$

satisfying the condition that the dominance metric, if evaluated for all solutes, should sum to unity:

$$\sum_{\alpha=1}^N D^\alpha = 1. \tag{4}$$

Intuitively, if D^α for a solute α is found to be close to 1 in a system, this implies $D^\beta \approx 0$ for $\beta \neq \alpha$ and the system is effectively single-component. On the other hand, for a multi-component system, we expect D^α to be in the range of (0,1) for two or more solutes. The D^α metric can thus serve as a way to quantify the multi-component character of solutes in a system. It remains to show that D^α reflects the thermodynamics of the phase separation process.

The thermodynamic driving force is Δf, the free energy change of the whole system after phase separation (Figure 2c). Given a free energy density $f(\phi)$ of a system as a function of its composition ϕ^α, we can show that by limiting the dense phase volume fraction v to be small, equivalent to probing regions close to the dilute phase boundary, Δf is given by (SI section II)

$$\begin{aligned}\Delta f &= -\frac{1}{2}\sum_{\alpha=1}^N\sum_{\beta=1}^N v k^\alpha v k^\beta (\partial_\alpha \partial_\beta f)|_{\psi_-} + \mathcal{O}[(vk)^3] \\ &= -\frac{1}{2}\sum_{\alpha=1}^N\sum_{\beta=1}^N v k^\alpha v k^\beta \partial_\beta \mu_\alpha(\psi_-) + \mathcal{O}[(vk)^3]\end{aligned} \tag{5}$$

which is negative given all eigenvalues of the Hessian $\partial_\alpha \partial_\beta f$ are positive, since the system is locally stable near

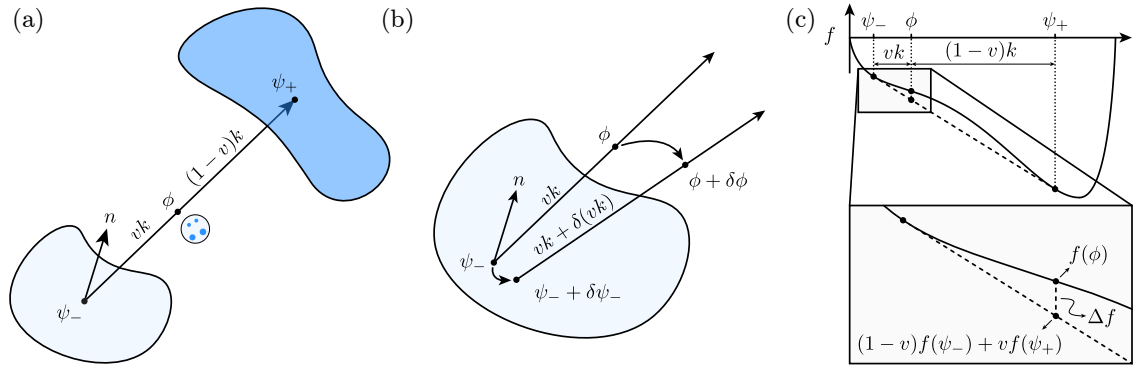

FIG. 2. **Geometrical construction of the phase space and its relation to thermodynamics.** (a) The full N-D phase space consists of dilute (light blue) and dense (dark blue) phase binodal boundaries, tie lines k^α connecting them, and dilute boundary surface normals n_α. (b) Experiments can probe the high-dimensional space by sampling two phase-separated points (ϕ^α and $\phi^\alpha + \delta\phi^\alpha$) and observing the response of the dilute phase $\delta\psi_-^\alpha$. (c) The free energy before and after phase separation is $f(\phi)$ and $(1-v)f(\psi_-) + vf(\psi_+)$ respectively, and a 1-D representation is used here but this is generalisable to any number of dimensions.

the binodal boundary. In the second line we used the expression for chemical potential $\mu_\alpha(\phi) = (\partial_\alpha f)|_\phi$. Since $vk^\alpha = \phi^\alpha - \psi_-^\alpha$ represents the phase space displacement of the total composition from the dilute composition, the sum over β can be viewed as computing the change in chemical potential of solute α under phase separation. We define the individual term

$$\Delta f^\alpha \equiv -\frac{1}{2} vk^\alpha \sum_{\beta=1}^{N} vk^\beta \partial_\beta \mu_\alpha(\psi_-) \tag{6}$$

such that if we form the ratio $\frac{\Delta f^\alpha}{\Delta f}$ we can write

$$\sum_{\alpha}^{N} \frac{\Delta f^\alpha}{\Delta f} = 1, \tag{7}$$

which is of a very similar form to Eq. (4). Indeed, by perturbing the equilibrium compositions we can show that $n_\alpha \propto \sum_{\beta=1}^{N} k^\beta (\partial_\alpha \partial_\beta f)|_{\psi_-}$ (SI section III) and as such, the equivalence of D^α and $\frac{\Delta f^\alpha}{\Delta f}$ can be established:

$$D^\alpha = \frac{\sum_{\beta=1} k^\alpha k^\beta (\partial_\alpha \partial_\beta f)|_{\psi_-}}{\sum_{\gamma=1}^{N} \sum_{\sigma=1}^{N} k^\gamma k^\sigma (\partial_\gamma \partial_\sigma f)|_{\psi_-}} = \frac{\Delta f^\alpha}{\Delta f}. \tag{8}$$

This validates D^α as a parameter grounded on thermodynamics. The physical interpretation of D^α is then the amount of stabilisation free energy contributed by solute α relative to that by all solutes, and this gives quantitative meaning to the assessment of a system being single or multi-component. Having established D^α as a valid dominance parameter, it is natural to investigate next how D^α responds to modulations of phase separation.

Poly(A)-RNA phase separates in the presence of PEG and high salt concentrations [21, 26] and we perform homotypic line-scans with 4% PEG (molecular weight 10 kilodaltons), and 800mM or 850mM of KCl (SI section IV). Dilute phase poly(A) concentrations are measured, so we use index 1 to denote poly(A) and index 2 for KCl, and we have $\Delta\phi^2 = 50$mM. Line-scan data (Figure 3a) shows a smaller R_1^1 after phase-separation at higher KCl. It is worth writing down the R_1^1 expression again:

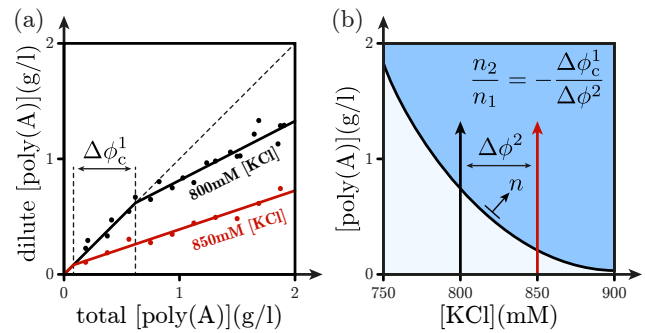

FIG. 3. **Modulation effect of KCl on poly(A) phase separation.** (a) Line-scan data for phase-separation of poly(A)-RNA in the presence of PEG and KCl. At higher [KCl] the increased charge screening allows inter-RNA interaction to be more favourable, leading to an increase in D^1 when [KCl] is increased. (b) Phase space illustration of the poly(A)-KCl cross-section.

$$R_1^1 = 1 - D^1 \tag{9}$$

so D^1 increases from 0.49 ± 0.05 to 0.66 ± 0.04. The increase in poly(A) dominance at higher KCl can be explained by the increased screening of negative backbone charges on poly(A), facilitating poly(A)-poly(A) interaction and rendering other interactions, for instance poly(A)-PEG, less significant. An interesting observation is that the onset of phase-separation shifts to a lower poly(A) concentration when salt concentration is increased, with $\Delta\phi_c^1 = -0.54 \pm 0.12$g/l. This can be inter-

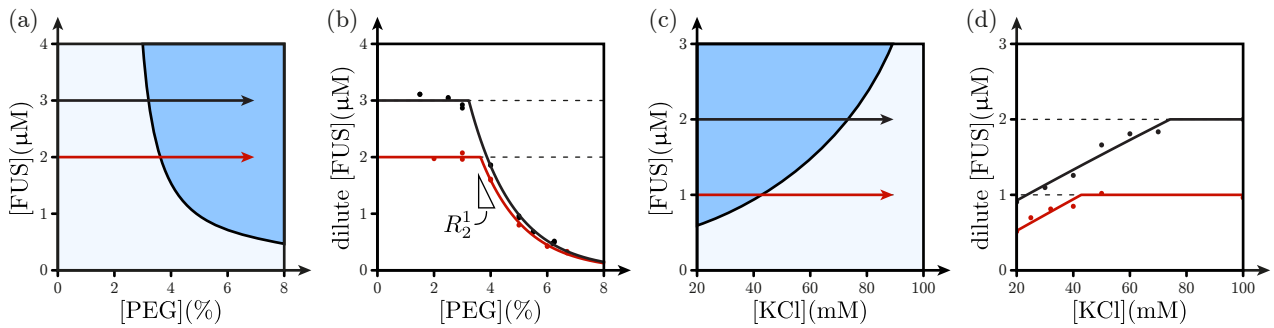

FIG. 4. **Heterotypic line-scans provide the same insights to the dominance formalism.** (a) Illustration of heterotypic line-scan sampling in a 2-D cross-section of the FUS-PEG phase space. Line-scans are performed at two fixed FUS concentrations, 3μM and 2μM. (b) Data from [19]. At low [PEG] no phase separation is observed, so the dilute phase [FUS] is simply a constant. When the line-scan trajectory enters the phase separated region the dilute phase [FUS] starts decreasing, and this initial gradient is taken as R_2^1. (c) Phase space illustration of the FUS-KCl line-scans. KCl dissolves condensates, in contrast to PEG. (d) Data from [17]. Scatter points are data and solid lines are phenomenological fits. Dashed lines indicate trivial results in the absence of phase-separation.

preted as an increase in overall phase-separation propensity, consistent with the picture that poly(A)-poly(A) repulsion weakens with more salt. By combining $\Delta\phi^2$ with $\Delta\phi_c^1$ we can deduce the ratio of surface normals $\frac{n_2}{n_1}$ in the poly(A)-KCl plane (Figure 3b). By definition, $n_1\Delta\phi_c^1 + n_2\Delta\phi^2 = 0$ so

$$\frac{n_2}{n_1} = -\frac{\Delta\phi_c^1}{\Delta\phi^2} \tag{10}$$

and this gives $\frac{n_2}{n_1} = -\frac{\Delta\phi_c^1}{\Delta\phi^2} = 10.8 \pm 2.4\,\frac{\mathrm{g/l}}{\mathrm{M}}$. By combining this with D^1, we can further estimate the ratio of tie line components, $\frac{k^1}{k^2}$, even though we have not explicitly measured any KCl concentration.

We construct the quantity $K_2^1 \equiv \frac{n_2}{n_1}\frac{D^1}{1-D^1}$, and using Eq. (3) we arrive at (SI section V)

$$K_2^1 \equiv \frac{n_2}{n_1}\frac{D^1}{1-D^1} = \frac{k^1}{k^2}\left[\frac{1}{1+\sum_{\alpha=3}^{N} D^\alpha/D^2}\right] \tag{11}$$

and to leading order, K_2^1 provides an approximation of the ratio of tie line components $\frac{k^1}{k^2}$. For the poly(A) system, we use the average of the D^1 and arrive at an approximate tie line component ratio of 9.4 ± 1.8g/l of poly(A) per 1M of KCl, so KCl partitions into poly(A) condensates. This is in essence the tie line estimation method used in [19] (SI section V). Terms in the square bracket of Eq. (11) represent the deviation of K_2^1 from $\frac{k^1}{k^2}$, and in a true 2-component system we expect $D^\alpha = 0$ for $\alpha = 3, 4, \ldots, N$, from which we have exactly $K_2^1 = \frac{k^1}{k^2}$. By assuming the dominance of a typical solute falls within the $(0, 1)$ range the corrections do not change the sign of K_2^1, so K_2^1 provides a easy way of assessing whether the solute 2 is partitioning into $\left(\frac{k^1}{k^2} > 0\right)$ or out of $\left(\frac{k^1}{k^2} < 0\right)$ condensates. Notably, this partitioning information becomes accessible without directly measuring the solute 2, giving our approach a high degree of flexibility. An important corollary arising from Eq. (11) is that given $0 < D^\alpha < 1$, the sign of K_2^1 is entirely determined by the sign of $\frac{n_2}{n_1}$, and thus the sign of $\frac{k^1}{k^2}$ can be deduced by simply observing the effect of the solute 2 on condensates. To put this in practical terms, if solute 2 dissolves condensates $\left(\frac{n_2}{n_1} < 0\right)$ it partitions out of condensates $\left(\frac{k^1}{k^2} < 0\right)$ and vice versa, provided that D^α falls within 0 and 1. This makes intuitive sense since it suggests that condensate-favouring modulators partition into condensates while condensate-disfavouring modulators are excluded from condensates. It is important however to point out here that some D^α can fall outside the 0 and 1 range. A subtle point here in calculating the tie line component ratio involving KCl is that the dissociation of the salt into K^+ and Cl^- means that KCl is not a single solute, and the line-scan is not traversing parallel to one axis but at an angle between two axes corresponding to K^+ and Cl^-, so mixing them is equivalent to performing a rotation of the two axes. This does not affect $D^1 = \frac{n_1 k^1}{\sum_{\gamma=1}^{N} n_\gamma k^\gamma}$ since the denominator is coordinate-independent and the numerator is not affected. Furthermore, since k^α and ϕ^α transform in the same way the measured K_2^1 represents the summed partitioning of K^+ and Cl^-. Converting between units and mixing solutes are both examples of general coordinate transformations in the phase space, and the geometrical nature of the theoretical construction allows these to be treated rigorously.

The homotypic line-scan discussed is a natural path towards conceptualising D^1, while in experiments the line-scan can also be performed by varying the concentration

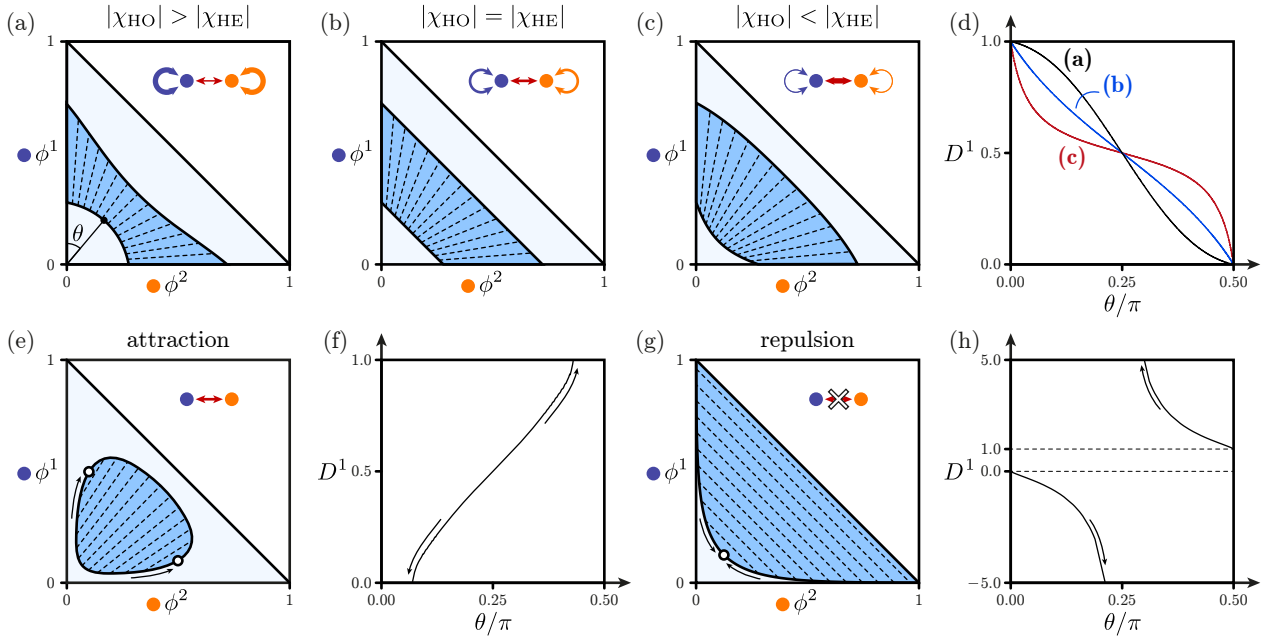

FIG. 5. **Computational model to illuminate the connection between D^1 and full phase space.** (a) to (c) Full phase diagrams of a simple ternary system computed using the Flory-Huggins free energy, where each solute phase-separates on their own and are coupled by a heterotypic interaction. Red solid lines are binodal boundaries and dashed red lines are tie lines. The definition of θ is illustrated in (a). (b) When the heterotypic attraction is the same as homotypic attractions the two solutes are equivalent, resulting in a phase space with flat binodal boundaries along $\phi^1 + \phi^2 =$ const. lines. When the heterotypic attraction becomes (a) weaker or (c) stronger than the homotypic attraction the curvature of the boundaries change accordingly as studied before [27]. (d) Computed D^1 along the dilute phase boundary. At small θ the total composition is close to the ϕ^1 axis, and entropic effect impedes partitioning of ϕ^2 so ϕ^1 is dominant in all cases. As θ increases, D^1 decreases from 1 as ϕ^2 starts to participate in phase separation, and this decrease is slowest when χ_{HE} is weak (a) and fastest when χ_{HE} is stong (c). (e) to (h) When phase-separation is driven purely by heterotypic interactions, both attraction (e) and repulsion (g) can lead to de-mixing. White points are critical points, and computed D^1 values are plotted in (f) and (h) respectively. As the point of evaluation approaches the critical points (black arrows) the D^1 value encounters a singularity as ΔF goes to 0. An interesting observation in (h) is that here, D^1 takes on values not in the range of $(0, 1)$, reflecting the abnormal behaviour of a repulsion-driven phase-separating system. All interaction parameters can be found in Appendix VI.

of a solute $2 \neq 1$. The relevant response is

$$R_2^1 = -\frac{n_2}{n_1} D^1. \tag{12}$$

This is termed the heterotypic line-scan, and has already been applied in the past to study tie lines through Eq. (11) [17, 19], and here we make the connection to D^1 using the same datasets. We take two sets of data: FUS-PEG from [19] and FUS-KCl from [17]. In both cases dilute phase FUS protein (index 1) concentration is measured, while the total concentrations of PEG or KCl is varied. In the FUS-PEG line-scan data from [19], two line-scans are performed at 2 and 3μM [FUS] while adding PEG up to 8% weight fraction. The dilute phase [FUS] measurements showed a plateau at low [PEG] and an exponential decrease as some thresholding [PEG] is reached (Figure 4a and 4b). The two points at the onset of the decrease are where the lines cross the phase boundary, and from these we estimate $\frac{n_2}{n_1} = 2.4 \pm 0.4 \frac{\mu M}{\%}$. The response function R_2^1 can be evaluated at the drop-off point as well, and since the $\frac{n_2}{n_1}$ measured corresponds to the average of the phase boundary gradient between 2 and 3 μM [FUS] we use the average gradient of the two line-scans at the onset of phase separation to obtain $R_2^1 = -1.58 \pm 0.06 \frac{\mu M}{\%}$. Finally, combining $\frac{n_2}{n_1}$ and R_2^1 we get $D^1 = -\frac{n_1}{n_2} R_2^1 = 0.65 \pm 0.12$. This value indicates there are other solutes actively participating in phase-separation and a likely candidate is PEG. This is also reflected in the fact that the FUS-PEG phase boundary measured using PhaseScan has strong dependence on [PEG] [28]. Substituting D^1 and $\frac{n_1}{n_2}$ into Eq. (11) gives $K_2^1 = 4.5 \pm 1.8 \frac{\mu M}{\%}$, providing an estimate of the relative partitioning between FUS and PEG. In the FUS-KCl system, KCl has the opposite effect compared to PEG as condensates are dissolved when more KCl is added to the system [17]. Line-scan data thus shows a steady increase of dilute phase [FUS] with increasing [KCl] (Figure 4c and 4d). We fit the dilute phase [FUS] after phase-separation using a linear function. Repeating the same calculations we obtain $\frac{n_2}{n_1} = -0.033 \pm 0.009 \frac{\mu M}{mM}$ and $R_2^1 = 0.020 \pm 0.003 \frac{\mu M}{mM}$ to give $D^1 = 0.61 \pm 0.24$, again

suggesting a FUS-dominated, multi-component system. The K_2^1 value obtained is $K_2^1 = -0.05 \pm 0.04 \frac{\mu\text{M}}{\text{mM}}$, implying overall salt is partitioning outside condensates. Heterotypic line-scans are thus an alternative to homotypic line-scans, and the two methods can have different signal-to-noise ratios depending on the phase space being probed. In general, for a solute α with a small D^α, heterotypic line-scans give more robust readouts and conversely, homotypic line-scan should be performed when D^α is large.

To provide a wholistic view of how D^α fits in the full phase space and changes along the phase boundary, we use a computational model to generate full phase spaces and compute individual D^α and explore how it changes with solute concentrations as well as with interaction strengths. We use the 2-component Flory-Huggins model [29, 30] as the free energy density and generate full phase diagrams with the convex hull algorithm [31–33] (Appendix VI). Following a previous study [27], we choose our interaction parameters such that the two solutes, ϕ^1 and ϕ^2, have the same homotypic interaction strength χ_{HO} that allows them to phase-separate on their own. We couple these solutes with an heterotypic interaction χ_{HE}, and it is chosen to be slightly weaker than (Figure 5a), the same as (Figure 5b), or slightly stronger than (Figure 5c) χ_{HO}. The dilute phase binodal boundary exhibits a changing sign in curvature as the heterotypic interaction is tuned [27]. For each point on the dilute phase boundary we compute the angle θ made between the vector connecting the origin to that point and the ϕ^1 axis. We compute D^1 directly (Appendix VI), and plot it as a function of θ for easy visualisation (Figure 5d). Since ϕ^1 phase-separates on its own, D^1 takes on the value of 1 in all three cases at $\theta = 0$. As ϕ^2 is added to the system, ϕ^2 also contributes to the phase-separation so D^1 decreases from 1. This decrease is slowest when χ_{HE} is of smaller magnitude than χ_{HO} as ϕ^1 still prefers to interact with itself and the phase-separation is predominantly ϕ^1-driven. When the heterotypic attraction increases, the decrease in D^1 becomes faster as $\phi^1 - \phi^2$ attraction increases in significance as expected. Another interesting case to observe is where the phase-separation is driven purely by the heterotypic interaction. As established before [19], phase-separation can happen with either strong heterotypic attraction (Figure 5e) or heterotypic repulsion (Figure 5g) in the absence of any homotypic interaction. Repeating the D^1 calculation gives drastically different results compared to cases before (Figure 5f and 5h). With strong heterotypic attraction, the computed D^1 starts off at a small value and increases as more ϕ^2 is added. This effect is of entropic origin: at low ϕ^2, the translational entropy of ϕ^2 acts as the main free energy barrier against phase-separation, and as ϕ^2 increases this barrier rapidly diminishes in size due to the logarithmic scaling of the entropic free energy. The interaction free energy is however only changing slowly, so the interaction free energy previously counterbalanced by the entropic free energy is suddenly released. Consequently, the free energy release by ϕ^2 is more significant compared to that by ϕ^1 and thus D^2 attains a much larger value than D^1. Conceptually, the dominance then also reflects which solute is 'limiting' in the phase separation process. With heterotypic repulsion, defining dense and dilute phases is non-trivial because the solutes partition into separate phases. Here we focus on the region of phase space where $\theta > \pi/4$ so that the dense phase is higher in ϕ^1. In this region, $D^1 > 1$ throughout and this implies $D^2 = 1 - D^1 < 0$. This can appear counter-intuitive, as it appears that ϕ^2 is in an energetically less favourable state after phase-separation. This is explained by the fact that by phase-separating, the change in chemical potential of ϕ^1 due to partitioning of ϕ^2 releases much more free energy to balance out the unfavourable contribution from ϕ^2 itself, and thus ϕ^2 is acting as a 'sacrificial' component. This behaviour is expected of real crowders [16, 34] but has so far not been observed in bio-molecular condensate systems. It is also worth noting that in both cases, as the system moves towards a critical point, D^1 appears to approach a singularity and this arises because at the critical point, $\Delta f = 0$ and the metric becomes ill-defined.

Motivated by the computational models, we finally outline experimental insights that can be gained if multiple solutes can be measured post phase separation. If D^α and ratios of n_α and k^α can be measured at each experimental point, entries in the Hessian $\partial_\alpha \partial_\beta f(\psi_-)$ can be obtained as well, which correspond to interaction energies of solutes in the dilute phase. This is based on the observation that $n_\alpha \propto \sum_{\beta=1}^N k^\beta \partial_\alpha \partial_\beta f(\psi_-)$. To illustrate the point, suppose $\partial_\alpha \partial_\beta f(\psi_-)$ consists of two terms: a constant, symmetric interaction energy matrix $\chi_{\alpha\beta}$ and a diagonal entropic term $\text{diag}\left(\frac{1}{L^1\psi_-^1}, \frac{1}{L^2\psi_-^2}, \ldots, \frac{1}{L^N\psi_-^N}\right)$, where L^α are sizes of the solute molecules. In doing so the free energy from translational entropy of solute α is assumed to be $\frac{\psi_-^\alpha}{L^\alpha} \ln \psi_-^\alpha$. Treating the interaction matrix and sizes L^α as unknowns, we have $N(N+1)/2 + N = \frac{1}{2}N^2 + \frac{3}{2}N$ fitting parameters. On the other hand, at each point ψ_-^α, we can form $N-1$ linearly independent equations using ratios of n_α's, so for an N-component system by sampling $\sim \frac{1}{2}N$ points, the interaction constants $\chi_{\alpha\beta}$ and molecular sizes L^α can be deduced. Practical implementation of this procedure can however be difficult, given the possibly large number of relevant solutes, but the prospect of obtaining $\chi_{\alpha\beta}$ in the dilute solution not only helps with understanding phase separation but also illuminates protein interactions in general, and can be a highly promising direction for further research.

To summarise, we construct an experimentally-accessible, dimensionless parameter D^α to quantify the dominance of solutes in a binary phase separation

system. The origin of D^α can be traced back to the phase space structure and the thermodynamics. We outline the data processing method using published results and illustrate the utility of D^1 in a practical poly(A) system. Combined with the dilute phase boundary surface normal n_α we further show that the dominance formulation enables approximate tie line component ratios to be easily determined without the need to measure all solute concentrations. The connection between the dominance and both homotypic and heterotypic responses are discussed, and the framework is further complemented by a computational model that illuminates the composition-dependent nature of the dominance parameter. This dependence stems from variations in the entropic barrier across the phase space. Last but not least we outline how measuring more solutes in a system might enable energetics and entropic parameters to be determined. Our work paves the way for systematic, quantitative studies of phase separation in the future.

Acknowledgement. The authors thank Mina Farag for helpful discussions. The research leading to these results has received funding from Global Research Technologies, Novo Nordisk A/S (H.A., T.P.J.K.), the European Research Council under the European Union's Horizon 2020 research and innovation programme through the Marie Skłodowska-Curie grant MicroREvolution (agreement ID 101023060; T.S.), the Newman Foundation (T.S., T.P.J.K.), and the European Research Council under the European Union's Horizon 2020 research and innovation program through the ERC grant DiProPhys (agreement ID 101001615; T.P.J.K.).

Conflict of interests. The authors declare no conflict of interests.

[1] J. W. Gibbs, American Journal of Science and Arts **16**, 441 (1874).

[2] S. F. Banani, H. O. Lee, A. A. Hyman, and M. K. Rosen, Nature Reviews Molecular Cell Biology **18**, 285 (2017).

[3] Y. Shin and C. P. Brangwynne, Science **357**, aaf4382 (2017).

[4] G. L. Dignon, R. B. Best, and J. Mittal, Annual Review of Physical Chemistry **71**, 53 (2020).

[5] C. P. Brangwynne, C. R. Eckmann, D. S. Courson, A. Rybarska, C. Hoege, J. Gharakhani, F. Jülicher, and A. A. Hyman, Science **324**, 1729 (2009).

[6] B. A. Gibson, L. K. Doolittle, M. W. Schneider, L. E. Jensen, N. Gamarra, L. Henry, D. W. Gerlich, S. Redding, and M. K. Rosen, Cell **179**, 470 (2019).

[7] A. Aulas, G. Caron, C. G. Gkogkas, N. V. Mohamed, L. Destroismaisons, N. Sonenberg, N. Leclerc, J. Alex Parker, and C. V. Velde, Journal of Cell Biology **209**, 73 (2015).

[8] J. Guillén-Boixet, A. Kopach, A. S. Holehouse, S. Wittmann, M. Jahnel, R. Schlüßler, K. Kim, I. R. Trussina, J. Wang, D. Mateju, I. Poser, S. Maharana, M. Ruer-Gruß, D. Richter, X. Zhang, Y.-T. Chang, J. Guck, A. Honigmann, J. Mahamid, A. A. Hyman, R. V. Pappu, S. Alberti, and T. M. Franzmann, Cell **181**, 346 (2020).

[9] J. E. Henninger, O. Oksuz, K. Shrinivas, I. Sagi, G. LeRoy, M. M. Zheng, J. O. Andrews, A. V. Zamudio, C. Lazaris, N. M. Hannett, T. I. Lee, P. A. Sharp, I. I. Cissé, A. K. Chakraborty, and R. A. Young, Cell **184**, 207 (2021).

[10] S. Ray, N. Singh, R. Kumar, K. Patel, S. Pandey, D. Datta, J. Mahato, R. Panigrahi, A. Navalkar, S. Mehra, L. Gadhe, D. Chatterjee, A. S. Sawner, S. Maiti, S. Bhatia, J. A. Gerez, A. Chowdhury, A. Kumar, R. Padinhateeri, R. Riek, G. Krishnamoorthy, and S. K. Maji, Nature Chemistry **12**, 705 (2020).

[11] A. Patel, H. O. Lee, L. Jawerth, S. Maharana, M. Jahnel, M. Y. Hein, S. Stoynov, J. Mahamid, S. Saha, T. M. Franzmann, A. Pozniakovski, I. Poser, N. Maghelli, L. A. Royer, M. Weigert, E. W. Myers, S. Grill, D. Drechsel, A. A. Hyman, and S. Alberti, Cell **162**, 1066 (2015).

[12] A. Bremer, M. Farag, W. M. Borcherds, I. Peran, E. W. Martin, R. V. Pappu, and T. Mittag, Nature Chemistry (2021), 10.1038/s41557-021-00840-w.

[13] M. Kar, F. Dar, T. J. Welsh, L. T. Vogel, R. Kühnemuth, A. Majumdar, G. Krainer, T. M. Franzmann, S. Alberti, C. A. Seidel, T. P. Knowles, A. A. Hyman, and R. V. Pappu, Proceedings of the National Academy of Sciences of the United States of America **119**, 1 (2022).

[14] A. Villois, U. Capasso Palmiero, P. Mathur, G. Perone, T. Schneider, L. Li, M. Salvalaglio, A. DeMello, S. Stavrakis, and P. Arosio, Small (2022), 10.1002/smll.202202606.

[15] J. P. Brady, P. J. Farber, A. Sekhar, Y. H. Lin, R. Huang, A. Bah, T. J. Nott, H. S. Chan, A. J. Baldwin, J. D. Forman-Kay, and L. E. Kay, Proceedings of the National Academy of Sciences of the United States of America **114**, E8194 (2017).

[16] A. Testa, M. Dindo, A. A. Rebane, B. Nasouri, R. W. Style, R. Golestanian, E. R. Dufresne, and P. Laurino, Nature Communications **12**, 1 (2021).

[17] H. Ausserwoger, D. Qian, G. Krainer, T. J. Welsh, T. Sneideris, T. M. Franzmann, S. Qamar, J. Nixon-Abell, M. Kar, P. S. G. Hyslop, A. A. Hyman, S. Alberti, R. V. Pappu, and Tuomas P. J. Knowles, bioRxiv (2023).

[18] A. A. André and E. Spruijt, International Journal of Molecular Sciences **21**, 1 (2020).

[19] D. Qian, T. J. Welsh, N. A. Erkamp, S. Qamar, J. Nixon-Abell, G. Krainer, P. St. George-Hyslop, T. C. T. Michaels, and T. P. J. Knowles, Physical Review X **12**, 041038 (2022), arXiv:2022.02.22.481401 [10.1101].

[20] A. A. André, N. A. Yewdall, and E. Spruijt, Biophysical Journal **122**, 397 (2023).

[21] N. Erkamp, M. Farag, D. Qian, T. Sneideris, T. Welsh, H. Ausserwoger, D. Weitz, R. Pappu, and T. Knowles, , 1 (2023), arXiv:2023.01.12.523837.

[22] J. A. Riback, L. Zhu, M. C. Ferrolino, M. Tolbert, D. M. Mitrea, D. W. Sanders, M. T. Wei, R. W. Kriwacki, and C. P. Brangwynne, Nature **581**, 209 (2020).

[23] M. T. Wei, Y. C. Chang, S. F. Shimobayashi, Y. Shin, A. R. Strom, and C. P. Brangwynne, Nature Cell Biology **22**, 1187 (2020).

[24] G. Krainer, T. J. Welsh, J. A. Joseph, J. R. Espinosa, S. Wittmann, E. de Csilléry, A. Sridhar, Z. Toprakcioglu, G. Gudiškytė, M. A. Czekalska, W. E. Arter, J. Guillén-Boixet, T. M. Franzmann, S. Qamar, P. S. George-Hyslop, A. A. Hyman, R. Collepardo-Guevara, S. Alberti, and T. P. J. Knowles, Nature Communications **12**, 1085 (2021).

[25] P. Yang, C. Mathieu, R. M. Kolaitis, P. Zhang, J. Messing, U. Yurtsever, Z. Yang, J. Wu, Y. Li, Q. Pan, J. Yu, E. W. Martin, T. Mittag, H. J. Kim, and J. P. Taylor, Cell **181**, 325 (2020).

[26] N. A. Erkamp, T. Sneideris, H. Ausserwöger, D. Qian, S. Qamar, J. Nixon-Abell, P. St George-Hyslop, J. D. Schmit, D. A. Weitz, and T. P. J. Knowles, Nature Communications **14**, 684 (2023).

[27] M. Farag, W. M. Borcherds, A. Bremer, T. Mittag, and R. V. Pappu, (2023).

[28] W. E. Arter, R. Qi, N. A. Erkamp, G. Krainer, K. Didi, T. J. Welsh, J. Acker, J. Nixon-Abell, S. Qamar, J. Guillén-Boixet, T. M. Franzmann, D. Kuster, A. A. Hyman, A. Borodavka, P. S. George-Hyslop, S. Alberti, and T. P. J. Knowles, Nature Communications **13**, 7845 (2022).

[29] M. L. Huggins, The Journal of Chemical Physics **9**, 440 (1941).

[30] P. J. Flory, The Journal of Chemical Physics **10**, 51 (1942).

[31] D. D. Lee, J. H. Choy, and J. K. Lee, Journal of Phase Equilibria **13**, 365 (1992).

[32] S. Mao, D. Kuldinow, M. P. Haataja, and A. Košmrlj, Soft Matter **15**, 1297 (2019), arXiv:1810.03689.

[33] J. Wolff, C. M. Marques, and F. Thalmann, Physical Review Letters **106**, 1 (2011).

[34] J.-M. Choi, F. Dar, and R. V. Pappu, PLOS Computational Biology **15**, e1007028 (2019).